DOI: 10.1021/ma100530k

Macromolecules
ARTICLE

Enhanced Electrical Conductivity by Macromolecular Architecture: Hyperbranched Electroactive and Degradable Block Copolymers Based on Poly(ε-caprolactone) and Aniline Pentamer

Baolin Guo, Anna Finne-Wistrand, and Ann-Christine Albertsson*

Department of Fibre and Polymer Technology, School of Chemical Science and Engineering, Royal Institute of Technology, SE-100 44, Stockholm, Sweden

Received March 10, 2010; Revised Manuscript Received April 9, 2010

ABSTRACT: We present macromolecular architecture design as a useful tool to enhance the conductivity of degradable polymers. Linear and hyperbranched copolymers with electrical conductivity and biodegradability were synthesized by an "$A_2 + B_n$ ($n = 2, 3, 4$)" strategy using carboxyl-capped aniline pentamer (CCAP) and branched poly(ε-caprolactone)s (PCLs) by coupling reactions. A more hydrophilic surface and lower crystallinity of the doped emeraldine state of aniline pentamer (EMAP) copolymer was achieved compared with PCLs, and TGA results demonstrated that the CCAP contents in the copolymers were almost the same. The structure of the polymers was characterized by FT-IR, NMR, and SEC. Good electroactivity of the copolymers was confirmed by UV and cyclic voltammetry (CV), and CV showed three pairs of redox peaks. The hyperbranched copolymers had a higher conductivity than the linear ones. It is suggested that the higher conductivity of the hyperbranched copolymer is due to the ordered distribution of peripheral EMAP segments that more easily form a conductive network. Therefore, the conductivity of the polymers is improved and controlled by the macromolecular architecture.

Introduction

The macromolecular architecture greatly effects the performance of polymers. Polymers with the same molecular weight consisting of the same monomer may possess different thermal, mechanical, degradation, and biological properties because of their different architectures.[1−4] Our group has synthesized the linear, star-branched, and cross-linked networks of degradable polymers and has extensively investigated the effect of the architecture on the degradation product, degradation rate, and thermal and mechanical properties of these degradable polymers.[5−9] As one of the fourth class of polymer architecture after traditional types including linear, cross-linked, and branched architectures, the hyperbranched polymers (HBPs) usually exhibit properties such as multiple terminal groups and globular shape similar to those of dendrimers. HBPs are potentially promising materials because of their easy synthesis and purification so that they represent a cost-effective alternative for dendrimers in some applications.[10,11] HBPs can be synthesized by a one-step polymerization process, such as the step-growth polycondensation of AB_x monomer and the classical "$A_2 + B_n$" ($n \geq 3$) approach.[12−14] Hyperbranched or dendronized conducting polymers exhibit interesting properties compared with their linear counterparts and have recently attracted considerable attention as high-performance organic conductors,[15,16] as magnetic,[17] electrochromic, and [18] high dielectric materials,[19] and as organic−inorganic hybrid electrolytes.[20]

Degradable and resorbable synthetic polymers are widely used in the biomedical field, scaffold preparation, bone fixation, sutures, and drug delivery systems. Aliphatic polyesters of lactones and lactides play an important role in this field because of their good mechanical properties, hydrolyzability, and biocompatibility.[21−23] Homopolymer and copolymers of PCL, which are biocompatible, absorbable, and biodegradable, are some of the polymers widely used in medical applications.[24−26] PCL also possesses outstanding permeability, and the degradation product of PCL is nontoxic and metabolizable.[9,27] The disadvantages of PCL are its slow rate of degradation and its hydrophobicity, but those can be overcome by copolymerization or blending with other polymers.[28−30] The third-generation biomaterials are cell- and gene-activating materials designed to stimulate specific cellular responses at the molecular level.[31] Resorbable polymer systems with molecular modifications can arouse specific interactions between cell integrins and thereby adjust cell behavior. Recent studies have shown that electrical signals can regulate cellular activities, including cell adhesion, migration, proliferation, and differentiation of many kinds of cells.[32−35] The degradable electrically conducting polymers (DECPs) with the unique properties of being electrically conducting and degradable are therefore a new exciting area and are attracting much attention. For example, a novel electrically conducting and biodegradable polymer was synthesized by oligomers of pyrrole and thiophene connected together via ester linkages.[36] The linear triblock and multiblock copolymers were prepared using aniline pentamer (AP) and polylactide, which are biodegradable and electroactive and are also easily processed.[37,38] Recently, a novel cytocompatible, biodegradable and electroactive polymer was synthesized by introducing alternating quaterthiophene units and ester units into one macromolecule.[39] These copolymers overcome to some extent the disadvantage of the conducting polymers, such as nonprocessability, poor solubility, poor polymer-cell interaction, and hydrophobicity. However, the synthesis of DECPs is still a challenge.

We have synthesized two-, four- and six-armed branched copolymers with electroactive and biodegradable properties based on polylactides and carboxyl-capped aniline trimer (CCAT).[40] However, the copolymers had quite a low conductivity, probably because of their low CCAT content and the short conjugated length of CCAT. Our object is thus to employ the macromolecular structures to enhance and control the conductivity of the electroactive and

*To whom correspondence should be addressed. Tel: +46-8-790 8274. Fax: +46-8-20 84 77. E-mail: aila@polymer.kth.se.

 Published on Web 04/28/2010

degradable polymers, here exemplified by linear and hyperbranched copolymers based on PCLs and CCAP. We hypothesized that macromolecular architecture is a useful tool to improve the conductivity of the degradable polymer: the hyperbranched copolymer should exhibit a higher level of conductivity than the linear copolymer with the same conductive segment content because the ordered distribution of the AP segments on the periphery of the hyperbranched copolymer should mean a better chance to form a conductive network. It is anticipated that a higher level of conductivity could thus be obtained with a lower CCAP content by macromolecular design and thus reduce the toxicity of the degradable copolymer. These copolymers have a promising prospect for use as a neural or cardiovascular conducting tissue engineering material, which can conduct bioelectrical signals in the body.

Experimental Section

Materials. The ε-caprolactone (CL) from Aldrich was dried in CaH_2 for 48 h and then distilled under reduced pressure. Ethylene glycol (EG, Aldrich) was distilled under reduced pressure. Trimethylolpropane (TMP, Aldrich) was recrystallized from dried acetone and then dried for 24 h in a vacuum oven. Pentaerythritol (PEN, Aldrich) was sublimated under reduced pressure. Stannous octoate ($Sn(Oct)_2$, Aldrich) was dried over molecular sieves and stored under a nitrogen atmosphere before use. *p*-Phenylenediamine, succinic anhydride (SA), ammonium persulfate ($(NH_4)_2S_2O_8$), phenylhydrazine, ammonium hydroxide (NH_3OH), hydrochloric acid (HCl), *N*,*N*′-dicyclohexyl carbodiimide (DCC), 4-dimethylaminopyridine (DMAP), ethanol (EtOH), *N*-methyl-2-pyrrolidone (NMP), dimethyl sulphoxide (DMSO), diethyl ether, chloroform ($CHCl_3$), hexane, methanol, and 1,4-dioxane were all purchased from Aldrich and were used without further purification.

Synthesis of Carboxyl-Capped Aniline Pentamer (CCAP). CCAP was synthesized according to refs 38 and 41. CCAP in the emeraldine base state (EM) was obtained from the oxidative coupling of 4-oxo-4-(4-(phenylamino) phenylamino) butanoic acid and *p*-phenylenediamine with two equivalent amounts of $(NH_4)_2S_2O_8$ as oxidant. The leucoemeraldine state of aniline pentamer (LMAP) was obtained by reduction of EMAP by phenylhydrazine. ^{1}H NMR (400 MHz, DMSO-d_6, δ): 12.09 (s, 2H, −COOH), 9.70 (s, 2H, −NHCO−), 7.63 (d, 2H, −NH−), 7.52 (s, 2H, −NH−), 7.38 (d, 4H, Ar−H), 6.85−6.94 (m, 16H, Ar−H). ^{13}C NMR (100 MHz, DMSO-d_6, δa) 173.91 (−COOH), 169.20 (−NHCO−), 140.81 (Ar−C), 138.27 (Ar−C), 137.06 (Ar−C), 135.60 (Ar−C), 130.74 (Ar−C), 120.41 (Ar−C), 119.52 (Ar−C), 118.33 (Ar−C), 117.46 (Ar−C), 115.34 m, 30.86 ($-CH_2-$), 28.98 ($-CH_2-$). All of these results agree well with the refs 38 and 41.

Synthesis of Linear and Star-Shaped PCLs. PCLs with different arms were prepared by ring-opening polymerization[7,42] (ROP) as follows: the monomer (CL), initiator ($Sn(Oct)_2$), and co-initiator (EG, TMP, and PEN) were weighed and added to a silanized round-bottomed flask in a glovebox (Mbraun MB 150B-G-I) purged with nitrogen. The mixture was then put in an oil bath at 110 °C under a nitrogen atmosphere for 48 h. After the reaction, 10 mL of chloroform was added to the flask to dissolve the mixture, which was then precipitated in 300 mL of hexane/methanol (v/v 95:5) solution. After filtration, the product was dried in a vacuum oven at room temperature for 24 h. The polymer was then dissolved in $CHCl_3$ and reprecipitated three times. Finally, the copolymer was dried in an oven at 40 °C. Samples were designated 2a-PCL, 3a-PCL, and 4a-PCL, which denote a PCL co-initiated with EG, TMP, and PEN, respectively.

The NMR spectra of the different PCLs are show in Figure 1. 2a-PCL: ^{1}H NMR (400 MHz, $CDCl_3$, δ): 4.26 (s, 2H, $-CH_2-$ from EG), 4.03 (t, 2H, $-CH_2O-$), 3.65 (m, 2H, $-CH_2OH$), 2.28 (t, 2H, $-CH_2-$), 1.62 (m, 2H, $-CH_2-$), 1.37 (m, 2H, $-CH_2-$). 3a-PCL: ^{1}H NMR (400 MHz, $CDCl_3$, δ): 4.05 (t, 2H, $-CH_2O-$), 4.00 (s, 2H, $-CH_2-$ from TMP), 3.63 (m, 2H, $-CH_2OH$), 2.30 (t, 2H, $-CH_2-$), 1.64 (m, 2H, $-CH_2-$), 1.37 (m, 2H, $-CH_2-$), 0.88 (m, 2H, $-CH_3$ from TMP). 4a-PCL: ^{1}H NMR (400 MHz, $CDCl_3$, δ): 4.11 (s, 2H, $-CH_2-$ from PEN), 4.06 (t, 2H, $-CH_2-$), 3.64 (m, 2H, $-CH_2OH$), 2.31 (t, 2H, $-CH_2-$), 1.65 (m, 2H, $-CH_2-$), 1.38 (m, 2H, $-CH_2-$). 4a-PCL: ^{13}C NMR (100 MHz, $CDCl_3$, δ): 173.46 (−CO−), 64.07 ($-CH_2O-$), 62.45 ($-CH_2-$ from PEN), 34.06 ($-CH_2-$), 28.29 ($-CH_2-$), 25.47 ($-CH_2-$), 24.52 ($-CH_2-$).

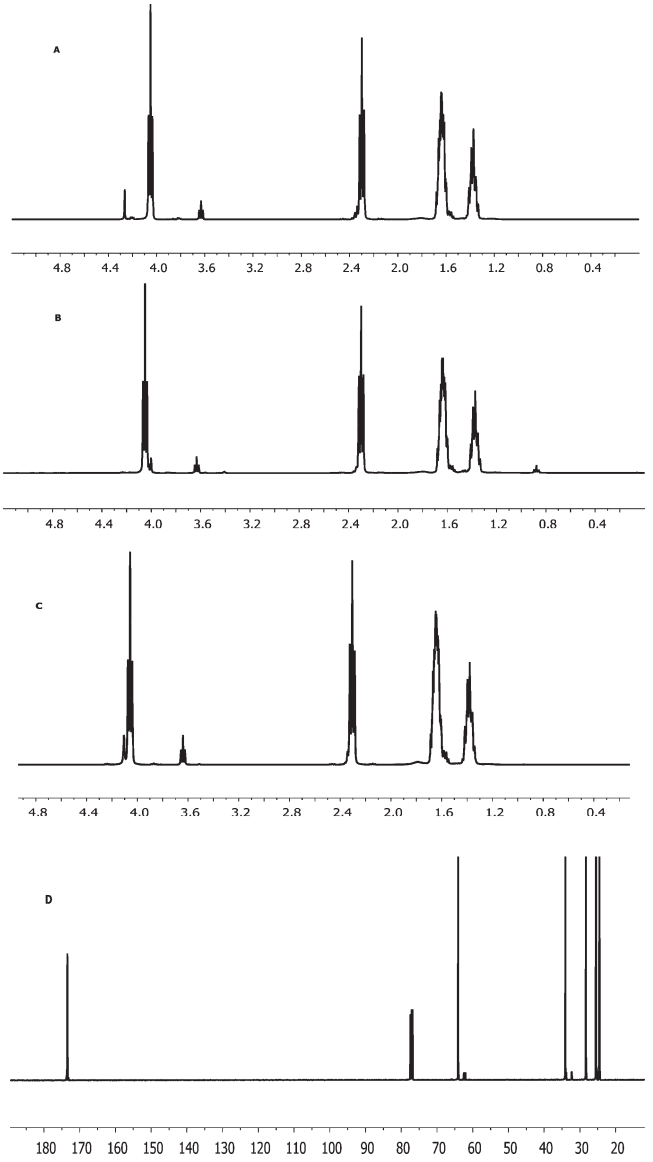

Figure 1. ^{1}H NMR spectra of the (A) 2a-PCL, (B) 3a-PCL, and (C) 4a-PCL, and (D) ^{13}C NMR spectrum of 4a-PCL.

Synthesis of Linear and Hyperbranched Copolymers. The synthesis of the copolymers using the "$A_2 + B_n$ (n = 2, 3, 4)" approach is shown in Scheme 1. Consider the synthesis of 4a-PCL LMAP copolymer as an example: Purified 4a-PCL (0.448 g) and CCAP (0.164 g) were dissolved in 10 mL of 1,4-dioxane and 2 mL of NMP mixture in a flame-dried flask with a magnetic stirrer under a nitrogen atmosphere, and DMAP (0.054 g) and DCC (0.264 g) were then added to the flask. The mixture was kept at 0 °C for 72 h. After the reaction, the mixture was filtered to remove dicyclohexylurea. The filtrate was precipitated in anhydrous diethyl ether. The copolymer was dissolved in chloroform and then again precipitated in anhydrous diethyl ether. The product obtained was dried in a vacuum oven for 48 h after filtration.

Scheme 1. Synthesis Route of the Linear and Hyperbranched Copolymers of PCLs and CCAP

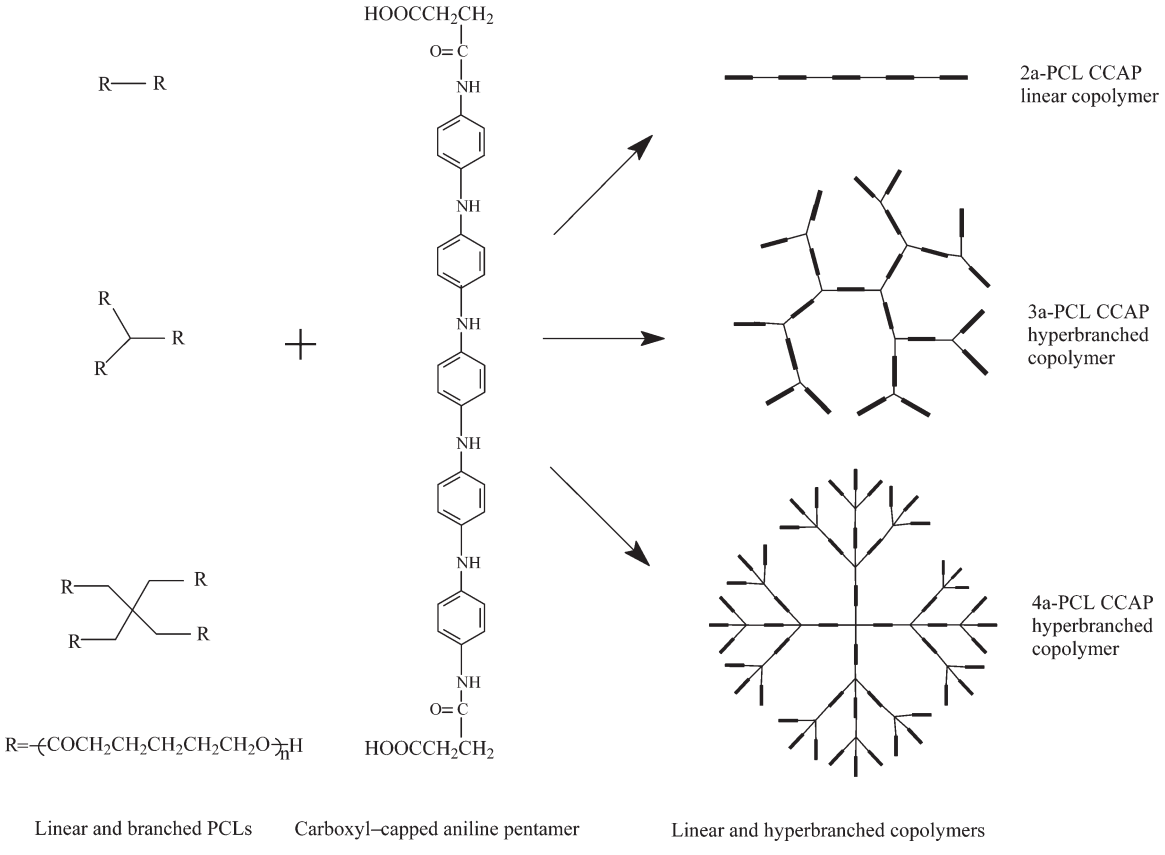

Characterization. FT-IR spectra of PCL, LMAP, and their copolymers were obtained with a Perkin Elmer Spectrum 2000 spectrometer (Perkin-Elmer Instrument) in the 4000−600 cm^{-1} range. Each spectrum was taken as the average of 20 scans at a resolution of 4 cm^{-1}.

^1H NMR (400 MHz) and ^{13}C NMR (100 MHz) spectra were obtained using a Bruker Avance 400 MHz NMR instruments with $CDCl_3$ as the solvent for all PCL samples and internal standard (δ 7.26 and 77.0). DMSO-d_6 was used as the solvent at room temperature and as internal standard (δ 2.50 and 39.5) for CCAP and all copolymer samples.

Size exclusion chromatography (SEC) was carried out using a TDA model 301 equipped with one or two GMH_{HR}-M columns with TSK-gel (Tosoh Biosep), a VE 5200 GPC autosampler, a VE 1121 GPC solvent pump and a VE 5710 GPC degasser, all of which were from Viscotek Corp. THF was used as the mobile phase (flow rate 1.0 mL/min). The measurement was carried out at 35 °C. The SEC apparatus was equipped with a triple detector array, including a differential refractive index, differential viscometer, and RALLS detector. A linear polystyrene standard was used for the calibration of the SEC apparatus.

The UV−vis spectra of oxidation process of copolymers solutions with trace oxidant were recorded on a UV−vis spectrophotometer (UV-2401).

The crystallization temperature (T_c), melting temperature (T_m), and crystallinity (X_c) of the polymers were assessed by differential scanning calorimetry (DSC) using a Mettler-Toledo DSC 820 module under a nitrogen atmosphere (nitrogen flow rate of 50 mL/min). Measurements were made during the first heating scan from 25 to 100 °C, which was held for 2 min to erase the thermal history, the first cooling from 100 to −70 °C and the second heating scan from −70 to 100 at 10 °C/min. Data for T_c and T_g were taken from the second heating scan. The crystallinity of the copolymers was calculated using the equation $X_c = \Delta H_f/H_f^0$, where X_c is the crystallinity, ΔH_f is the heat of fusion of the sample, and ΔH_f^0 is the heat of fusion of 100% crystalline PCL. The value of ΔH_f^0 used for the calculations was 139.5 J/g.[43]

Thermogravimetric analysis (TGA) was used to determine the ratio of PCL to CCAP, and the thermal stability of the polymers. TGA was carried out under a nitrogen atmosphere (nitrogen flow rate 50 mL/min) and a heating rate of 10 °C/min. The scan range was from 30 to 800 °C.

Cyclic voltammetry (CV) of CCAP and its copolymers was carried out on an electrochemical workstation interfaced and monitored with a PC computer. A three-electrode system with a platinum disk as working electrode (surface area 0.14 cm^2), a platinum-wire as auxiliary electrode, and an Ag/AgCl as reference electrode was employed. The scan rate was 60 mV/s. The sample was dissolved in a DMSO/1 mol/L HCl mixture. All solutions were deoxygenated for 10 min with nitrogen prior to the electrochemical measurements. The electrical conductivity of the 1 mol/L HCl doped EMAP copolymer films was determined by the standard Van Der Pauw four-probe method. The conductivity of each sample was measured four times at different current values, and the average value was taken as the conductivity of the sample.

The surface hydrophilicity of the PCLs and copolymer films was estimated by water contact angle measurements (CAMs) using a contact angle and surface tension meter (KSV instruments). A drop of Mini-Q water was placed on the surface of the sample, and the image of the water drop was recorded by a digital camera. The images were then analyzed with KSV software to obtain the contact angle. The contact angle of each sample was taken as the average of five measurements at different points on the samples.

Results and Discussion

Synthesis of PCLs. PCLs with different branched structures (2a-PCL, 3a-PCL, and 4a-PCL) were synthesized by ROP. $Sn(Oct)_2$ was used as initiator, with monomer-to-initiator ratio of 10 000:1, and the tin residuals were therefore very low after purification.[44] Figure 1 shows the ^1H NMR of (A) 2a-PCL,

Table 1. Properties of the PCLs

sample code	reaction time (h)	monomer conversion (%)[a]	M_n (g/mol)[b]	M_n (g/mol)[c]	MWD[c]	M_n theory (g/mol)[d]
2a-PCL	48	98.3	2400	3250	1.09	2800
3a-PCL	48	99.3	4300	4700	1.14	4200
4a-PCL	48	99.6	5600	6200	1.12	5500

[a] Calculated from ^{1}H NMR on crude reaction mixture. [b] Determined by ^{1}H NMR [c] Number-average molecular weight and distribution determined by SEC [d] Theoretical number- = average molecular weight, $M_n = [M]/[I]_{co} \times M_{CL} \times$ Conversion

(B) 3a-PCL, and (C) 4a-PCL and (D) the ^{13}C NMR spectrum of 4a-PCL. All ^{1}H NMR data are listed in the experimental part. It is noted that the spectra contained not only the CL peaks but also the signal from the co-initiator. For example, the $-CH_2-$ (δ 4.11) of the co-initiator PEN appears in the ^{1}H NMR spectrum (Figure 1C), and this is confirmed in the ^{13}C NMR spectrum of 4a-PCL (Figure 1D), the signal of PEN appearing at 64.2 ppm. Therefore, these polymers with star-shaped structures are certainly obtained. The hydroxyl group (δ 3.65) at the PCL chain end is used for the coupling reaction with CCAP in the next step. The same trends were found for the EG and TMP systems.

We determined monomer conversion of the PCLs by comparing the peak integrals of methylene protons in PCL (about δ 4.04 in Figure 1) with those of the monomer CL (δ 4.20 in Figure 1), and the results are summarized in Table 1. The conversion of all systems was quite high, exceeding 98% after 48 h of reaction, which indicated that the low ratio of $Sn(Oct)_2$ to monomer had a high catalytic activity. We calculated molecular weights of the PCLs by comparing the peak integrals of methylene protons (δ 4.04, $-CH_2-$ in Figure 1) with those of the methylene protons next to the terminal hydroxyl groups (δ 3.65, $-CH_2OH$ in Figure 1). The molecular weights calculated by NMR are also listed in Table 1. These results are very close to the theoretical values and agree well with the SEC results. Furthermore, they also had a very narrow MWD. All of these results indicated the successful synthesis of the PCLs with different numbers of branches.

Characterizations of the Linear and Hyperbranched Copolymers. The linear and hyperbranched copolymers were prepared by the "$A_2 + B_n$ (n = 2, 3, 4)" approach. The coupling condensation polymerization took place between the hydroxyl groups in the PCLs and the carboxyl groups in CCAP with the DCC as water condensation agent and DMAP as catalyst to form the different architectural copolymers. The chemical structures of the copolymers obtained were verified by FT-IR, NMR, and SEC. Figure 2 presents the FT-IR spectra of the LMAP copolymer (c) together with those of its corresponding precursors PCL (a), and LMAP (b). In Figure 2a, the characteristic absorption band at 1722 cm^{-1} is assigned to the C=O stretching mode, and the peak at 1166 cm^{-1} arising from the O−C−O of the PCL is also observed. The characteristic peaks at 1692 and 1650 cm^{-1} are assigned to the C=O stretching vibration in LMAP in Figure 2b, and the bands at 1610 and 1509 cm^{-1} are characteristic of the benzenoid ring of AP. There is no peak at 1587 cm^{-1} corresponding to the quinoid unit, indicating a successful reduction from the EMAP to LMAP. All characteristic absorption bands in both LMAP and PCL were observed in Figure 2c demonstrated that the target copolymer was obtained. There is a broad peak at ~3355 cm^{-1} corresponding to hydroxyl groups and amide groups in the copolymer, which can increase the hydrophilicity of the polymer.

The ^{1}H NMR and ^{13}C NMR spectra were used to confirm further the structure of the copolymers, as shown in Figure 3.

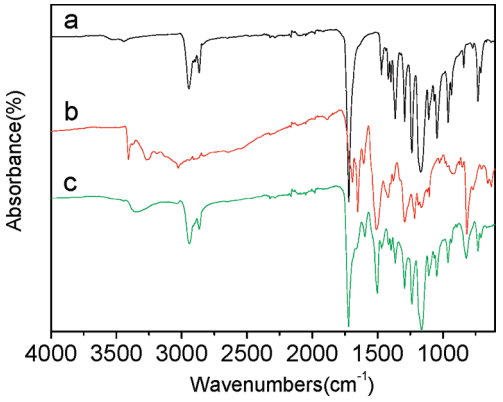

Figure 2. FT-IR spectra of (a) PCL, (b) LMAP, and (c) their copolymer.

Consider the ^{1}H NMR spectrum of 2a-PCL LMAP copolymer in DMSO-d_6 as an example: ^{1}H NMR (400 MHz, DMSO-d_6, δ): 1.38 (m, 2H, $-CH_2-$), 1.65 (m, 2H, $-CH_2-$), 2.31 (t, 2H, $-CH_2-$), 4.06 (t, 2H, $-CH_2-$), 4.24 (s, 2H, $-CH_2-$ from EG) for the PCL segment and 2.58−2.67 (m, 4H, $-CH_2CH_2-$), 6.84−6.95 (m, 16H, Ar−H), 7.39 (d, 4H, Ar−H), 7.54 (s, 2H, −NH−), 7.62 (d, 2H, −NH−), 9.72 (s, 2H, −NHCO−) for the LMAP segment. In Figure 3a, it can be seen that the methylene protons next to the terminal hydroxyl groups in PCL, which were observed at ~3.65 ppm in the ^{1}H NMR spectrum of PCL in Figure 1, were absent from the ^{1}H NMR spectrum of the copolymer (Figure 3a), indicating that the esterification reactions took place between the hydroxyl-capped 2a-PCL and the carboxyl group of CCAP. There was also a new peak at 172.2 ppm in the ^{13}C NMR spectrum of the linear copolymer in Figure 3b, which also confirms that esterification occurred between the PCL and CCAP. Compared with the single peak of the newly formed esterification peak and the amide group peak of the linear copolymer in Figure 3b, these newly formed esterification group peaks and the amide group (−NHCO−) peaks split into multiple peaks in Figure 3c,d of the hyperbranched copolymer because these groups are in different chemical environments of the subunit ("inner" or "outer" parts of the hyperbranched copolymer),[45,46] and this further demonstrated that the hyperbranched copolymers had been successfully synthesized.

The molecular weight and molecular weight distribution (MWD) values were recorded on a THF-SEC utilizing universal calibration, a method in which the apparatus is calibrated using both narrow and broad polystyrene standards. The molecular weight of the copolymers were 2.9 × 10^4 (MWD = 1.6), 2.4 × 10^4 (MWD = 3.4), and 2.7 × 10^4 (MWD = 2.9) for the 2a-PCL copolymer, 3a-PCL copolymer, and 4a-PCL copolymer, respectively. The relationship between intrinsic viscosity and molecular weight was studied using the Mark−Houwink equation $[\eta] = kM^{\alpha}$; the values of α are equal to 0.5 at the θ state and between 0.65 and 0.8 for linear random coils in the good solvent. However, it was found that for the 3a-PCL hyperbranched copolymer and the 4a-PCL hyperbranched copolymers, the α values were ~0.34, which is commonly below the value of 0.5 for branched polymers[47,48] and much lower than that for the 2a-PCL copolymers (α = 0.77). All of these results indicate a much smaller hydrodynamic size and a highly branched compact and globular structure of the hyperbranched copolymers.

Thermal Properties of the Polymers. The thermal properties were measured by DSC, and the T_c, T_m, and X_c of the polymers are listed in Table 2. The X_c of 2a-PCL, 3a-PCL,

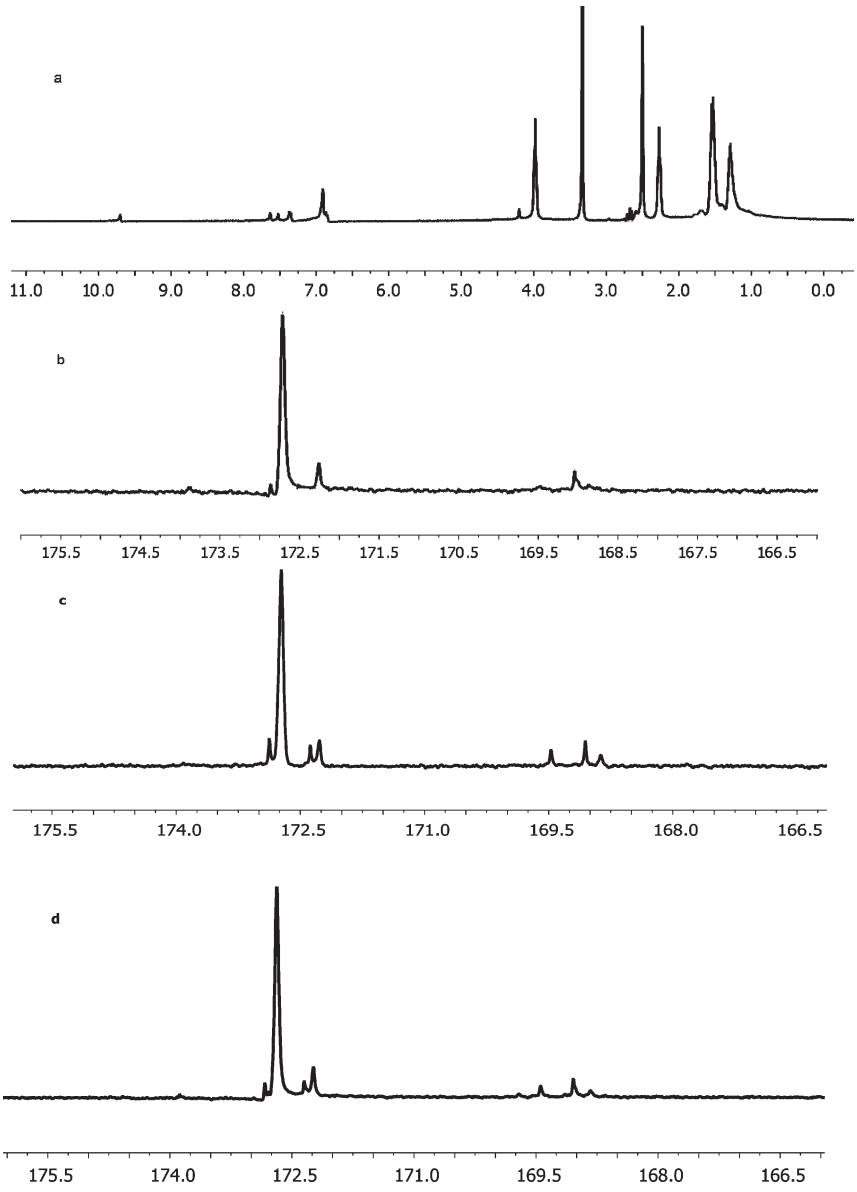

Figure 3. ^{1}H NMR of (a) 2a-PCL LMAP copolymer and the ^{13}C NMR spectra of (b) 2a-PCL LMAP copolymer, (c) 3a-PCL LMAP copolymer, and (d) 4a-PCL LMAP copolymer.

Table 2. T_c, T_m, and X_c of the Polymers

sample code	T_c (°C)	T_m (°C)	X_c
2a-PCL	35.0	52.2	52.3
3a-PCL	31.9	49.5	43.0
4a-PCL	25.0	41.3	37.2
2a-PCL EMAP copolymer	34.6	52.7	34.8
3a-PCL EMAP copolymer	27.8	49.5	29.3
4a-PCL EMAP copolymer	23.2	40.9	25.7

and 4a-PCL decreased sharply with increasing number of arms of the PCLs. This may be because the star-shaped core imposed restrictions on PCL crystallization.[49] The T_m of the 2a-PCL, 3a-PCL, and 4a-PCL decreased accordingly because of the difference in crystallinity and crystalline imperfections due to more free end groups in the more branched polymers. The parameter T_c is used to evaluate nucleation during polymer melt crystallization. The higher the T_c, the easier the stable nucleus can be formed via the regular arrangement of polymer segments, and the higher crystallizing ability of the polymer.[50] The 2a-PCL has the highest T_c, so it has the higher crystallizing ability and thus the highest X_c.

The T_c of the copolymers was a little lower than that of the corresponding PCLs, indicating a lower crystallization ability of the copolymer, probably because the PCL repeating unit nearest to the branched core was unable to crystallize and the chain folds were less tight in the hyperbranched copolymer,[49] whereas the rigid AP segment hindered the PCL segment from organizing and impeding the crystallization. The copolymer therefore has a much lower X_c than the counterpart PCLs. However, there seems to be no obvious difference between the T_m of the PCLs and their corresponding copolymers, and this can be explained by the better thermal stability of the CCAP segment in the copolymer.

Thermal stability of electroactive polymers is important in many applications. The thermal stability of the PCLs and their corresponding copolymers were tested by TGA and are shown in Figure 4. A small weight loss (~4%) from the PCLs and their copolymers occurred in the temperature range 100−220 °C, which was ascribed to water evaporation and to the loss of other solvents trapped in the polymers. In the case of the pure PCLs, there was a major weight loss between 230 and 450 °C, and the residual mass above 450 °C was

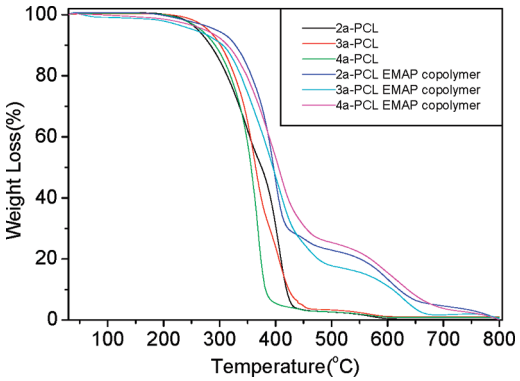

Figure 4. TGA curves of the PCLs and their EMAP copolymers.

Table 3. EMAP Content and Conductivity of the EMAP Copolymers

sample name	EMAP content (theoretical)	conductivity(S/cm)
2a-PCL EMAP copolymer	22.4 (25.0%)	5.01×10^{-6}
3a-PCL EMAP copolymer	21.8 (25.0%)	2.42×10^{-5}
4a-PCL EMAP copolymer	22.8 (25.0%)	8.02×10^{-6}

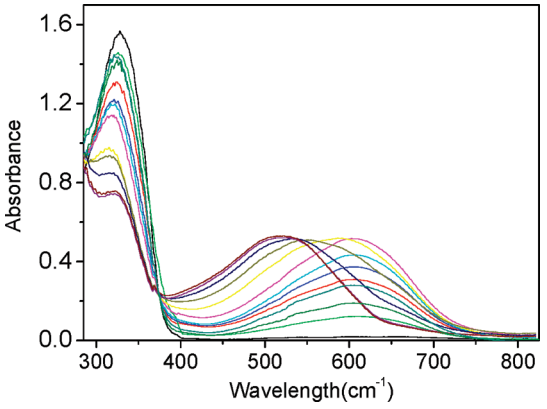

Figure 5. Chemical oxidization process of the LMAP copolymers with a trace amount of $(NH_4)_2S_2O_8$ in NMP solution.

almost 5%, indicating PCL main chain degradation. In the case of the EMAP copolymers, the first evident weight loss took place between 220 and ~450 °C, 72−74% of the weight of the copolymer being lost because of the PCLs main chain degradation. The greater thermal stability of the copolymer than of the pristine PCL is probably due to the greater thermal stability of the EMAP segments. The EMAP content in the copolymer can be calculated by using the TGA curves because the PCLs segments were almost completely degraded after 450 °C; the results are listed in Table 3. It was found that these results are close to the theoretical ones, and this confirms the successful synthesis of the copolymers. Between ~450 and 800 °C, there was another obvious weight loss of the copolymers related to the degradation of the EMAP segments. The LMAP copolymers have a thermal stability similar to that of the EMAP copolymers. All of these results demonstrated that these copolymers have an excellent thermal stability.

Electrochemical Properties of the Linear and Hyperbranched Copolymers. The electroactivity of the biomaterials means that they can transmit bioelectrical signals in vivo and play an important role in life activities. The electrochemical properties of the copolymer were characterized by UV and CV. Figure 5 shows the chemical oxidation of the copolymers in NMP solution. A trace amount of $(NH_4)_2S_2O_8$ was added to the 3a-PCL LMAP copolymer NMP solution. The solution gradually changed to blue and then to mauve because of the oxidation of the copolymer. The oxidation process was monitored by the UV absorbance spectrum and is plotted in Figure 5. The copolymer exhibits only one absorption peak at ~330 nm, which is attributed to the $\pi-\pi^*$ transition in the conjugated benzene unit. This also confirms the full reduction from EMAP to LMAP, as demonstrated by FT-IR. The absorption peak started to decrease in intensity and gradually underwent a blue shift during the oxidation. Meanwhile, a new absorption peak was developed at ~610 nm, which was assigned to an excitonic transition from the benzoid ring to the quinoid ring appeared in the spectrum and which continuously increased in intensity. The absorption peak at 610 nm began to undergo a blue shift (from 610 to 530 nm) after reaching its maximum intensity. The intensity increase and the blue shift of the peak at 610 nm during the oxidation process can be explained by the three-step oxidation of the copolymer (Scheme 2).

Scheme 2. Molecular Structure of CCAP Segment in the Copolymer at Various Oxidation States

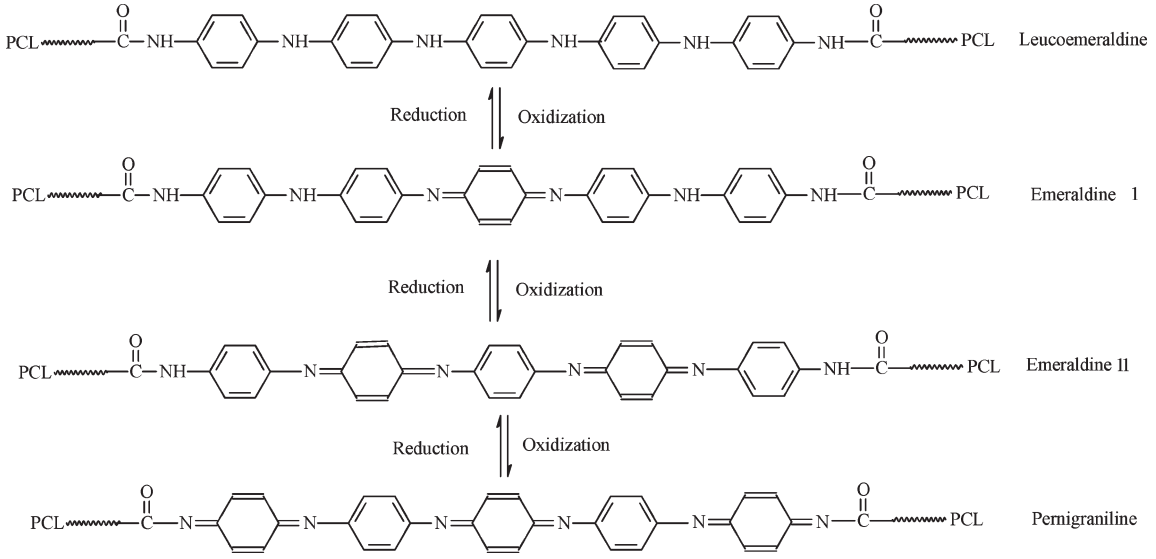

During the continuous oxidation of copolymer in the leucoemeraldine oxidation state, the copolymer reached the first emeraldine oxidation state (emeraldine I in Scheme 2), with each CCAP segment containing only one quinoid ring, which is why the UV spectrum showed the second absorption peak at 610 nm. The copolymer was then oxidized to the second emeraldine oxidation state (emeraldine II in Scheme 2), with each CCAP segment containing two quinoid rings, which increased the intensity of the absorption at 610 nm. Subsequently, the UV absorption exhibited a blue shift to ~530 nm after the absorption peak at 610 nm reached its maximum intensity, indicating that the pernigraniline oxidation state was formed.[51]

Figure 6 shows cyclic voltammograms for LMAP and their linear and hyperbranched copolymers in a DMSO/HCl mixture. The concentration was 0.25 wt % for LMAP and for all of the copolymers, and the concentration of HCl was 1 mol/L. The cyclic voltammograms of 2a-PCL LMAP copolymer (Figure 6b), 3a-PCL LMAP copolymer (Figure 6c), and 4a-PCL LMAP copolymer (Figure 6d) showed three pairs of redox peaks (0.26, 0.42, and 0.65 V), which is different from polyaniline, which typically shows two pairs of redox peaks.[52] The first well-defined oxidation peak at ~0.26 V can be attributed to the redox process from the "leucoemeraldine" to the "emeraldine I" form (Scheme 2), and the second oxidation peak at ~0.42 V is assigned to the transition from the "emeraldine I" to the "emeraldine II" state. At higher potentials, the oxidation peak at ~0.65 V is due to the transition from the "emeraldine II" state to the "pernigraniline" oxidation state (Scheme 2). These cyclic voltammograms for the copolymers are quite similar to that for the LMAP in Figure 6a. These three oxidation processes of the copolymers are in good agreement with UV absorption results, as shown in Figure 5. All of these UV spectroscopic and electrochemical results demonstrate the good electroactivity of the copolymers.

Electrical Conductivity of the Copolymers. The PCL EMAP copolymers were dissolved in chloroform and doped with the same amount of 1 mol/L HCl. The electrical conductivity values of the EMAP copolymer films were determined by the standard four probe method and are shown in Table 3. The conductivity of the copolymers was between 2.42×10^{-5} and 5.01×10^{-6} S/cm, which is much lower than that of AP films (10^{-2} S/cm). This is because of the introduction of nonconjugated PCL segments to the copolymers. However, this conductivity value is sufficient to conduct bioelectrical signals in vivo because the microcurrent intensity is also quite low in human body.[53]

In Table 3, the conductivity of the hyperbranched copolymers is higher than that of the linear copolymer, although these copolymers have almost the same EMAP content as that tested by TGA. The conductivity of 3a-PCL EMAP hyperbranched copolymer and 4a-PCL EMAP hyperbranched copolymer is, respectively, 4.8 and 1.6 times as high as that of the linear copolymer. In linear copolymer, the EMAP segments are isolated by PCL chains, and it is difficult for AP segments to form a network for electron transport from one polymer chain to another (Scheme 3). Furthermore, a microphase separation can occur as a result of a self-assembly process among the linear block copolymers.[38] The soft PCL segments can easily aggregate together, contributing to a continuous matrix, whereas the hard AP segments form discontinuous domains. An AP domain benefits electric conduction, but a tunnel effect through the PCL matrix has to take place between two neighboring domains to achieve electric conduction. Therefore, the apparent conductivity is comparatively low in the case of the linear copolymer. In the hyperbranched copolymers, the peripheral EMAP segments are distributed in an orderly manner to some extent due to the special structure of the hyperbranched copolymers. Because of the strong interaction between the EMAP segments in the solvent, the EMAP segments can aggregate together and easily form an intricate network of EMAP, which promote electric conduction (Scheme 3). There is thus a much greater possibility of forming a conductive intricate network of EMAP segments in the hyperbranched copolymer than in the linear copolymer with the same EMAP content. The conductivity of the

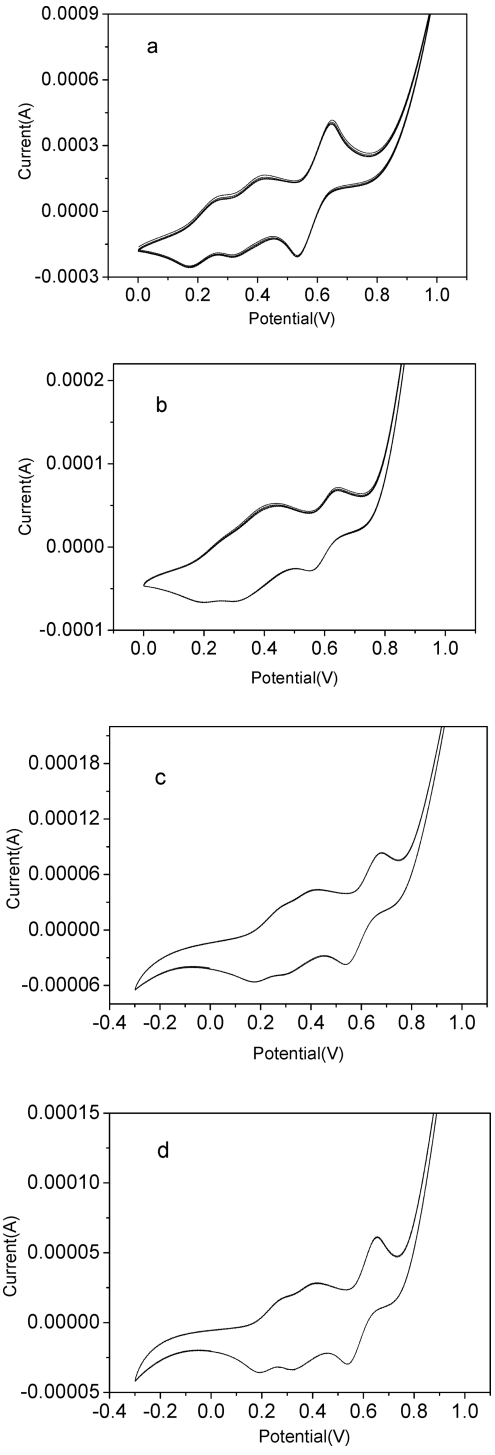

Figure 6. Cyclic voltammograms for (a) LMAP, (b) 2a-PCL LMAP copolymer, (c) 3a-PCL LMAP copolymer, and (d) 4a-PCL LMAP copolymer in a DMSO/HCl mixture.

Scheme 3. Proposed Model for the Higher Conductivity of Hyperbranched Copolymers with That of the Linear Copolymers with the Same EMAP Content

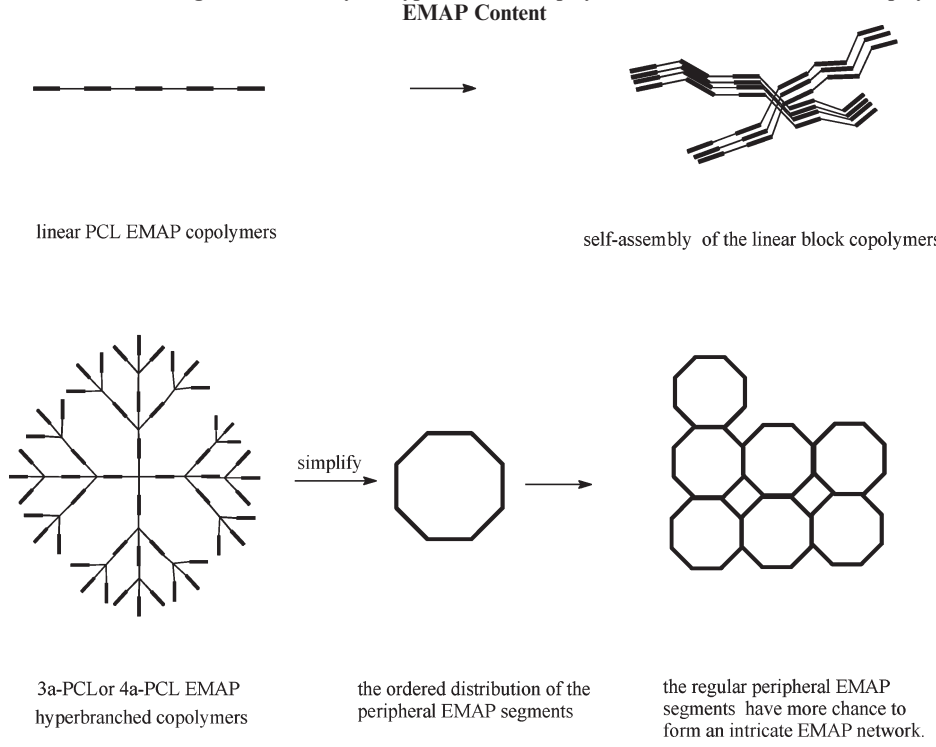

3a-PCL copolymer is higher than that of the 4a-PCL copolymer, which may be because the 4a-PCL copolymer has more defects than the 3a-PCL copolymer because of its overcrowded branches. We can therefore use macromolecular architecture to improve the conductivity of the polymers. This is especially important in the biomedical field because a high concentration of CCAP in the polymer is toxic. We can now design a hyperbranched copolymer or dendrimer to give a higher conductivity with a lower AP content and thus reduce the toxicity of the polymers.

Wettability of the Polymers. Surfaces with a moderate hydrophilicity (30−60°) have been shown to be optimal for cell adhesion, proliferation, and function.[54,55] The surface wettability of the PCLs and copolymers in different oxidation state was determined, and the results are shown in Figure 7. Water contact angles of PCLs were ~60°, and the differences between the different architectures are quite small. The 2a-PCL has a higher water contact angle than the 3a-PCL and 4a-PCL because of its higher crystallinity. These values are a little lower than that of the ref 56, which is 66°, because of the lower molecular weight of the PCLs with more hydroxyl groups in the polymers. The PCL LMAP copolymers have somewhat higher water contact angle than the pure PCLs, which may be because of the high hydrophobicity of LMAP segments. The contact angles of PCL EMAP copolymers were lower than those of the corresponding PCL LMAP copolymers because the hydrophilicity of the AP segment in the EM state was higher than that in the LM state. The dramatic decrease to ~30° of the water contact angle of the PCL EMAP copolymers doped with 1 mol/L HCl indicated that the polymer surface became much more hydrophilic as a result of the formation of the emeraldine salt. Increasing the hydrophilicity of the material would involve lowering the surface energy, and this would greatly influence the interactions between the cell and material surfaces when in contact.[57] These medium hydrophilic surfaces are better for cell adhesion and cell proliferation.

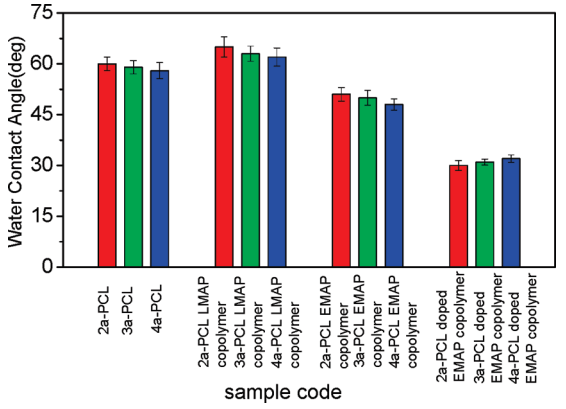

Figure 7. Water contact angles of the polymers.

Conclusions

Macromolecular architecture design has been demonstrated as a tool to increase the conductivity of polymers. The higher electrical conductivity of the hyperbranched copolymers compared with that of the linear copolymers with the same conductive content was achieved by macromolecular architecture. This has significant meaning in tissue engineering because the same level of conductivity can be obtained by macromolecular engineering with a lower concentration of the conductive segment and thus reduces the toxicity of the DECPs. This is the first example of hyperbranched copolymers with electroactive and degradable properties. The wettability of the doped EMAP copolymer increased dramatically, and the X_c of the copolymers decreased sharply compared with the values for pristine PCLs, and this means that the disadvantages of PCL, such as hydrophobicity and low degradation rate can be overcome. Their structures and properties have been fully characterized by FT-IR, ^{1}H NMR, ^{13}C NMR, SEC, DSC, TGA, UV, CV, and CAM. These copolymers have excellent thermal stability with a two-step thermal degradation behavior and good electroactive properties with a three-step

oxidation/reduction process. These linear and hyperbranched electrically conductive copolymers with biodegradability have a great potential for application in neural or cardiovascular tissue engineering, and these results open the way to obtaining enhanced electrical conductivity of the polymers by macromolecular architectural design.

Acknowledgment. We are grateful to the Swedish Research Council (grant no. 2008-5538), the China Scholarship Council (CSC), and The Royal Institute of Technology (KTH) for financial support for this work. We also thank Assoc. Prof. Ann Maria Cornell and M.Sc. Simon Leijonmarck for CV and conductivity measurements.

References and Notes

(1) Tomalia, D. A. *Prog. Polym. Sci.* **2005**, *30*, 294–324.
(2) Finne, A.; Albertsson, A. C. *Biomacromolecules* **2002**, *3*, 684–690.
(3) Nasongkla, N.; Chen, B.; Macaraeg, N.; Fox, M. E.; Frechet, J. M. J.; Szoka, F. C. *J. Am. Chem. Soc.* **2009**, *131*, 3842−3843.
(4) Fox, M. E.; Szoka, F. C.; Frechet, J. M. J. *Acc. Chem. Res.* **2009**, *42*, 1141–1151.
(5) Srivastava, R. K.; Albertsson, A. C. *Macromolecules* **2006**, *39*, 46–54.
(6) Finne, A.; Albertsson, A. C. *J. Polym. Sci., Part A: Polym. Chem.* **2003**, *41*, 1296–1305.
(7) Numata, K.; Srivastava, R. K.; Finne-Wistrand, A.; Albertsson, A. C.; Doi, Y.; Abe, H. *Biomacromolecules* **2007**, *8*, 3115–3125.
(8) Hoglund, A.; Odelius, K.; Hakkarainen, M.; Albertsson, A. C. *Biomacromolecules* **2007**, *8*, 2025–2032.
(9) Hakkarainen, M.; Hoglund, A.; Odelius, K.; Albertsson, A. C. *J. Am. Chem. Soc.* **2007**, *129*, 6308–6312.
(10) Konkolewicz, D.; Gray-Weale, A.; Perrier, S. *J. Am. Chem. Soc.* **2009**, *131*, 18075−18077
(11) Jikei, M.; Kakimoto, M. *Prog. Polym. Sci.* **2001**, *26*, 1233–1285.
(12) Voit, B. I.; Lederer, A. *Chem. Rev.* **2009**, *109*, 5924–5973.
(13) Hao, J. J.; Jikei, M.; Kakimoto, M. A. *Macromolecules* **2002**, *35*, 5372–5381.
(14) Gao, C.; Yan, D. *Prog. Polym. Sci.* **2004**, *29*, 183–275.
(15) Wang, F.; Rauh, R. D.; Rose, T. L. *J. Am. Chem. Soc.* **1997**, *119*, 11106–11107.
(16) Miller, L. L.; Duan, R. G.; Tully, D. C.; Tomalia, D. A. *J. Am. Chem. Soc.* **1997**, *119*, 1005–1010.
(17) Spetseris, N.; Ward, R. E.; Meyer, T. Y. *Macromolecules* **1998**, *31*, 3158–3161.
(18) Wang, F.; Wilson, M. S.; Rauh, R. D.; Schottland, P.; Thompson, B. C.; Reynolds, J. R. *Macromolecules* **2000**, *33*, 2083–2091.
(19) Yan, X. Z.; Goodson, T. *J. Phys. Chem. B* **2006**, *110*, 14667–14672.
(20) Liao, C. C.; Wu, H. Y.; Saikia, D.; Pan, Y. C.; Chen, Y. K.; Fey, G. T. K.; Kao, H. M. *Macromolecules* **2008**, *41*, 8956–8959.
(21) Parrott, M. C.; Benhabbour, S. R.; Saab, C.; Lemon, J. A.; Parker, S.; Valliant, J. F.; Adronov, A. *J. Am. Chem. Soc.* **2009**, *131*, 2906–2916.
(22) Albertsson, A. C.; Varma, I. K. *Biomacromolecules* **2003**, *4*, 1466–1486.
(23) Varma, I. K.; Albertsson, A. C.; Rajkhowa, R.; Srivastava, R. K. *Prog. Polym. Sci.* **2005**, *30*, 949–981.
(24) Lee, C. C.; Grayson, S. M.; Frechet, J. M. J. *J. Polym. Sci., Part A: Polym. Chem.* **2004**, *42*, 3563–3578.
(25) Kweon, H.; Yoo, M. K.; Park, I. K.; Kim, T. H.; Lee, H. C.; Lee, H. S.; Oh, J. S.; Akaike, T.; Cho, C. S. *Biomaterials* **2003**, *24*, 801–808.
(26) van der Ende, A. E.; Kravitz, E. J.; Harth, E. *J. Am. Chem. Soc.* **2008**, *130*, 8706–8713.
(27) Hakkarainen, M.; Adamus, G.; Hoglund, A.; Kowalczuk, M.; Albertsson, A. C. *Macromolecules* **2008**, *41*, 3547–3554.
(28) Riva, R.; Schmeits, S.; Jerome, C.; Jerome, R.; Lecomte, P. *Macromolecules* **2007**, *40*, 796–803.
(29) Koning, C.; van Duin, M.; Pagnoulle, C.; Jerome, R. *Prog. Polym. Sci.* **1998**, *23*, 707–757.
(30) Srivastava, R. K.; Albertsson, A. C. *Macromolecules* **2007**, *40*, 4464–4469.
(31) Hench, L. L.; Polak, J. M. *Science* **2002**, *295*, 1014−1017.
(32) Wong, J. Y.; Langer, R.; Ingber, D. E. *Proc. Natl. Acad. Sci. U.S.A.* **1994**, *91*, 3201–3204.
(33) Zhao, M.; Bai, H.; Wang, E.; Forrester, J. V.; McCaig, C. D. *J. Cell Sci.* **2004**, *117*, 397–405.
(34) Guimard, N. K.; Gomez, N.; Schmidt, C. E. *Prog. Polym. Sci.* **2007**, *32*, 876–921.
(35) Quigley, A. F.; Razal, J. M.; Thompson, B. C.; Moulton, S. E.; Kita, M.; Kennedy, E. L.; Clark, G. M.; Wallace, G. G.; Kapsa, R. M. I. *Adv. Mater.* **2009**, *21*, 4393−4397.
(36) Rivers, T. J.; Hudson, T. W.; Schmidt, C. E. *Adv. Funct. Mater.* **2002**, *12*, 33–37.
(37) Huang, L. H.; Zhuang, X. L.; Hu, J.; Lang, L.; Zhang, P. B.; Wang, Y. S.; Chen, X. S.; Wei, Y.; Jing, X. B. *Biomacromolecules* **2008**, *9*, 850–858.
(38) Huang, L. H.; Hu, J.; Lang, L.; Wang, X.; Zhang, P. B.; Jing, X. B.; Wang, X. H.; Chen, X. S.; Lelkes, P. I.; MacDiarmid, A. G.; Wei, Y. *Biomaterials* **2007**, *28*, 1741–1751.
(39) Guimard, N. K. E.; Sessler, J. L.; Schmidt, C. E. *Macromolecules* **2009**, *42*, 502–511.
(40) Guo, B. L.; Finne-Wistrand, A.; Albertsson, A. C. *Biomacromolecules* **2010**, *11*, 855–863.
(41) Chen, L.; Yu, Y. H.; Mao, H. P.; Lu, X. F.; Zhang, W. J.; Wei, Y. *Chem. J. Chin. Univ.* **2004**, *25*, 1768–1770.
(42) Dong, C. M.; Qiu, K. Y.; Cu, Z. W.; Feng, X. D. *Macromolecules* **2001**, *34*, 4691–4696.
(43) Andronova, N.; Finne, A.; Albertsson, A. C. *J. Polym. Sci., Part A: Polym. Chem.* **2003**, *41*, 2412–2423.
(44) Stjerndahl, A.; Wistrand, A. F.; Albertsson, A. C. *Biomacromolecules* **2007**, *8*, 937–940.
(45) Jikei, M.; Chon, S. H.; Kakimoto, M.; Kawauchi, S.; Imase, T.; Watanebe, J. *Macromolecules* **1999**, *32*, 2061–2064.
(46) Lin, Y.; Gao, J. W.; Liu, H. W.; Li, Y. S. *Macromolecules* **2009**, *42*, 3237–3246.
(47) Turner, S. R.; Voit, B. I.; Mourey, T. H. *Macromolecules* **1993**, *26*, 4617–4623.
(48) Lin, Q.; Long, T. E. *Macromolecules* **2003**, *36*, 9809–9816.
(49) Nunez, E.; Ferrando, C.; Malmstrom, E.; Claesson, H.; Werner, P. E.; Gedde, U. W. *Polymer* **2004**, *45*, 5251–5263.
(50) Zhao, Y.; Keroack, D.; Prud'homme, R. *Macromolecules* **1999**, *32*, 1218–1225.
(51) Chao, D. M.; Ma, X. B.; Lu, X. F.; Cui, L. L.; Mao, H.; Zhang, W. J.; Wei, Y. *Macromol. Chem. Phys.* **2007**, *208*, 658–664.
(52) Shreepathi, S.; Holze, R. *Chem. Mater.* **2005**, *17*, 4078–4085.
(53) Niple, J. C.; Daigle, J. P.; Zaffanella, L. E.; Sullivan, T.; Kavet, R. *Bioelectromagnetics* **2004**, *25*, 369–373.
(54) Andrade, J. D.; King, R. N.; Gregonis, D. E.; Coleman, D. L. *J. Polym. Sci., Polym. Symp.* **1979**, 313–336.
(55) Edlund, U.; Kallrot, M.; Albertsson, A. C. *J. Am. Chem. Soc.* **2005**, *127*, 8865–8871.
(56) Cheng, Z. Y.; Teoh, S. H. *Biomaterials* **2004**, *25*, 1991–2001.
(57) Brunius, C. F.; Edlund, U.; Albertsson, A. C. *J. Polym. Sci., Part A: Polym. Chem.* **2002**, *40*, 3652–3661.